

# Strain-Driven “Sinusoidal” Valley Control of Hybridized $\Gamma$ – K Excitons

Yingtong Zhu,<sup>1</sup> Kang Lan,<sup>1</sup> Shiling Li,<sup>1</sup> Ning Hao,<sup>2</sup> Ping Zhang,<sup>1,3</sup> and Jiyong Fu<sup>1,\*</sup>

<sup>1</sup>Department of Physics, Qufu Normal University, Qufu 273165, Shandong, China

<sup>2</sup>Anhui Province Key Laboratory of Low-Energy Quantum Materials and Devices,

High Magnetic Field Laboratory, HFIPS, Chinese Academy of Sciences, Hefei, Anhui 230031, China

<sup>3</sup>Beijing Computational Science Research Center, Beijing 100084, China

The photoluminescence (PL) of momentum-indirect  $\Gamma$ –K excitons in monolayer  $WS_2$  under biaxial strain was recently observed by Blundo *et al.* [Phys. Rev. Lett. **129**, 067402 (2022)], yet its microscopic origin remains elusive. Here we develop a unified framework that reproduces the measured PL and reveals its fundamental excitonic mechanism. We reveal that: (i) the PL originates from genuinely hybridized direct-indirect excitonic *eigenstates*, rather than *nominally* mixed species with fixed dominant character; (ii) the direct exciton converts into the indirect one via a previously unrecognized two-step pathway—exchange-interaction-driven exciton transfer followed by a spin flip; and (iii) a higher-energy indirect exciton, absent from prior studies, acts as a crucial *intermediate* mediating this conversion. Beyond explaining experiment, our theory predicts a striking strain-driven “sinusoidal” valley response, furnishing a continuously tunable *valley dial* that far exceeds binary control schemes. This unified picture of strain-engineered direct-indirect exciton dynamics introduces a new paradigm for manipulating long-lived valley degrees of freedom, opening a pathway toward programmable valley pseudospin engineering and next-generation valleytronic quantum technologies.

**Introduction.**— Monolayer transition-metal dichalcogenides (TMDCs) have emerged as a versatile platform for exploring excitonic and valleytronic phenomena in two dimensions [1, 2]. Owing to their strong Coulomb interactions [3, 4] and reduced dielectric screening, these materials host tightly bound excitons in diverse configurations, including momentum-direct (bright or spin-forbidden dark) [5–10] and indirect (momentum-forbidden dark) [11–13] states. The coexistence and coupling of these direct and indirect species offer a unique window into spin-valley interactions. Understanding how these states evolve under external engineering knobs—such as strain [13–16]—is essential for tailoring light-matter interactions and exciton dynamics in TMDC-based valleytronic devices.

Recent experiments, supported by the first-principles calculations [11] have uncovered clear photoluminescence (PL) signatures of indirect  $\Gamma$ –K excitons in monolayer  $WS_2$ . However, interpretation based on *nominally* mixed direct or indirect excitons, where each state retains one fixed dominant component, fails to capture the observed peak behavior or its strain dependence. Moreover, the microscopic pathway that transfers population between direct and indirect species remains unresolved. Given the inherently long lifetime of indirect excitons and their potential application for coherent quantum control, a unified theoretical model incorporating strain-mediated PL, valley polarization (VP), and the full set of intra- and intervalley relaxation channels is highly desirable—for both fundamental understanding and the realization of strain-programmable valley pseudospin functionalities.

Here, we bridge this gap by developing a unified framework that captures the strain, thermal, and magnetic responses of both direct and indirect excitons, achieving excellent agreement with experiment [Fig. 1(e)]. We show that the observed PL originates from hybridized excitonic *eigenstates* rather than *nominally* mixed species. We further identify a two-step conversion mechanism—exchange interaction fol-

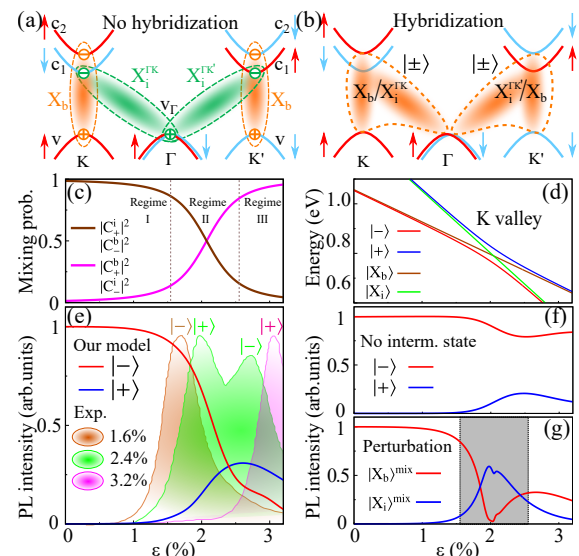


Figure 1. (Color online) (a) Spin-valley configurations of the direct exciton ( $X_b$ ) and momentum-indirect excitons ( $X_i^{\Gamma K}$ ,  $X_i^{K \Gamma}$ ), involving the spin-split CB branches ( $c_1, c_2$ ), the upper VB ( $v$ ), and the  $\Gamma$ -valley VB ( $v_{\Gamma}$ ). (b) Schematic hybridization between  $X_b$  and  $X_i$  forming the eigenstates  $|\pm\rangle$ . (c) Strain dependence of mixing coefficients  $C_{\pm}$  and  $C_{\pm}^2$ , with the dominant component of  $|\pm\rangle$  interchanging near  $\varepsilon \approx 2\%$ . (d) Strain evolution of excitonic energies. (e–g) PL intensity vs strain: (e) full model (red/blue) compared with experimental data [shaded (purple, green, pink) regions] from Ref. [11]; (f) model without the intermediate state; (g) perturbative approach, with the shaded (gray) region [referring to Regime II in (c)] marking where the perturbation breaks down.

lowed by spin flip—and uncover a previously unrecognized higher-energy state that acts as a crucial *intermediate* mediating this conversion [Fig. 2]. Strikingly, our model predicts a robust “sinusoidal” VP control in the upper hybridized branch [Fig. 3(a)], enabling a continuously tunable *valley dial* far more versatile than binary control schemes. These results

establish a unified picture of strain-engineered valley physics, and introduce a new concept: “sinusoidal” valley control, opening a pathway for leveraging long-lived indirect excitons in valley information processing, logic operations, and next-generation valleytronic architectures.

*Model Hamiltonian.*— The spin-orbit coupling (SOC) endows TMDCs with spin-valley *locked* band structure at the K and K' valleys of the Brillouin zone [17–20]. The upper valence band (VB;  $v$ ) and two spin branches of the conduction band (CB)—lower ( $c_1$ ) and upper ( $c_2$ )—constitute the basis for direct excitons [Fig. 1(a)]: bright ( $X_b$ ) and dark ( $X_d$ ; spin-forbidden) excitons. With increasing strain, while the CB minimum remains at the K valley, the VB maximum shifts toward the  $\Gamma$  point ( $v_\Gamma$ ), driving a crossover from direct to indirect band gap [13, 21]. This evolution favors the conversion of direct ( $X_b$ ) into indirect ( $X_i$ ) excitons, where  $X_i^{\Gamma K}$  ( $X_i^{\Gamma K'}$ ) consists of an electron in the K (K') valley ( $c_1$ ) bound to a hole in the  $\Gamma$  valley [Fig. 1(a)]. We further introduce a previously unrecognized higher-energy indirect exciton  $X_m^{\Gamma K}$  ( $X_m^{\Gamma K'}$ ) [Fig. 2(a)] with electron residing in upper  $c_2$  band.

Symmetry analysis reveals that the direct-indirect excitonic hybridization between  $X_b$  and  $X_i$  occurs [11], through their shared electronic states residing in the same valley [Fig. 1(b)]. The resulting multiexcitonic Hamiltonian under the basis  $\{|X_b^K\rangle, |X_i^{\Gamma K}\rangle, |X_b^{\Gamma K'}\rangle, |X_i^{\Gamma K'}\rangle\}$  reads [11],

$$\mathcal{H} = \mathcal{E}_+ \varsigma_0 \otimes \tau_0 - \mathcal{E}_- \varsigma_z \otimes \tau_0 + \Delta \mathcal{E}_+ \varsigma_0 \otimes \tau_z - \Delta \mathcal{E}_- \varsigma_z \otimes \tau_z + \Delta_R \varsigma_x \otimes \tau_0 + \Delta_I \varsigma_y \otimes \tau_z, \quad (1)$$

where  $\varsigma_0$  ( $\tau_0$ ) is the identity matrix and  $\varsigma_{x,y,z}$  ( $\tau_{x,y,z}$ ) represents the Pauli (“pseudospin”) matrices acting within the exciton (valley) subspace. We define  $\mathcal{E}_\pm = (E_{X_b}^0 \pm E_{X_i}^0)/2$  and  $\Delta \mathcal{E}_\pm = (\Delta E_{X_b} \pm \Delta E_{X_i})/2$ , in which  $E_j^0$  is the zero-field ( $B = 0$ ) energy of  $X_j$  and  $\Delta E_j = (1/2)g_j \mu_B B$  represents valley-Zeeman shift, with  $g_j$  the  $g$  factor ( $j = X_b, X_i$ ). The parameter  $\Delta = \Delta_R + i\Delta_I$  characterizes the hybridization (coupling) between  $X_b$  and  $X_i$  with  $\Delta_R$  ( $\Delta_I$ ) the real (imaginary) components.

*Multi-excitonic energies with strain and magnetic responses.*— We adopt the two-band model proposed by Xiao *et al.* [18] to determine the single-particle band edges. We then incorporate many-body interactions to obtain the excitonic binding energies by solving the Bethe-Salpeter equation (BSE) [1, 22–26], where the exciton state is expressed as  $\Psi_n = \sum_{c,v,\mathbf{k}} J_{c,v,\mathbf{k}}^{(n)} |v\mathbf{k} \rightarrow c\mathbf{k}\rangle$ , with  $c$  ( $v$ ) denoting the conduction (valence) band,  $\mathbf{k}$  the wave vector, and  $J$  the BSE expansion coefficient. To further refine the single-particle states for evaluating many-body corrections, we employ an 11-band tight-binding model that includes second-nearest-neighbor hopping terms [27, 28]. With these considerations, we obtain the zero- $B$ -field energy of  $X_b$  and  $X_i$ ,

$$E_{X_b}^0 = E_g + \frac{1}{2} \Delta_c - \frac{1}{2} \Delta_v - V_{X_b} + \delta_{X_b} \epsilon, \quad (2)$$

$$E_{X_i}^0 = E_g + \frac{1}{2} \Delta_c - \Delta_\Gamma - V_{X_i} + \delta_{X_i} \epsilon, \quad (3)$$

where  $\Delta_\Gamma$  is the  $\Gamma - K$  VB offset. We consider the exciton binding energies as  $V_{X_b} = V_{X_i} = \langle V_{e-h} \rangle$ , the expectation value

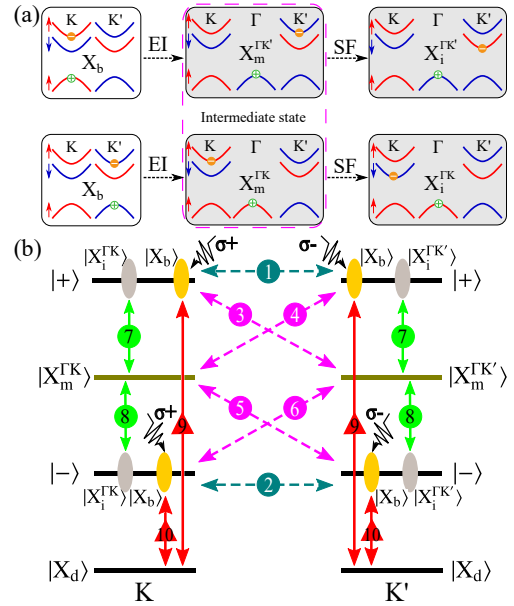


Figure 2. (Color online) (a) Upper: Transition pathway from the direct exciton  $X_b$  in the K valley to the indirect exciton  $X_i^{\Gamma K'}$  in the K' valley, mediated by exchange interaction [29] and spin flip, with  $X_m^{\Gamma K'}$  as the intermediate state. Lower: time-reversed counterpart of the upper panel. (b) Intra- (solid arrows, 7–10) and intervalley (dashed arrows, 1–6) relaxation channels among hybridized ( $|+\rangle, |-\rangle$ ) and non-hybridized ( $X_m, X_d$ ) excitonic states under linearly polarized excitation. The hybridized states contain direct (yellow) and indirect (gray) components. Double arrows denote reversible up- and down-conversion processes, with the latter energetically favored.

of the electron-hole Coulomb interaction from BSE. The last term in Eq. (2) [Eq. (3)] describes the strain-induced energy shift, which is approximately linear in the considered strain range [11], with the strain response coefficients  $\delta_{X_b}$  [ $\delta_{X_i}$ ].

To determine valley-Zeeman shifts, rather than invoking the empirical decomposition into spin, valley and atomic-orbital contributions [30], we treat valley and orbital components on equal footing via the orbital angular momentum  $\mathbf{L}$ , evaluated from first-principles calculations [31–34]. Namely, for a Bloch state  $|n\mathbf{k}\rangle$  the effective  $g$  factor is  $g_{n,\mathbf{k}} = L_{n,\mathbf{k}} + S_{n,\mathbf{k}}$ , giving the  $\tau$ -valley exciton energies under  $B$  field  $E_j^\tau(B) = E_j^0 + \tau \Delta E_j(B)$ ,  $j = X_b, X_i$ . For other excitonic energies, including the spin-forbidden dark ( $X_d$ ) and the higher-energy indirect ( $X_m$ ) excitons [Fig. 2(a)], see the Supplementary Material (SM). Note that, for notational simplicity, here the valley index of indirect exciton  $X_{i(m)}^{\Gamma K(K')}$  is assigned according to the electron constituent only, i.e.,  $X_{i(m)}^{\Gamma K(K')} \equiv X_{i(m)}^{K(K')}$ .

*Hybridized direct-indirect excitonic eigenstates and nominally mixed excitons.*— From Eq. (1), the hybridized “ $X_b/X_i$ ” eigenstates ( $|\pm\rangle$ ) in the K valley and the corresponding eigenenergies ( $E_{|\pm\rangle}$ ) are obtained as  $|\pm\rangle = C_\pm^b |X_b\rangle + C_\pm^i |X_i\rangle$  and  $E_{|\pm\rangle} = E_+ \pm \sqrt{E_-^2 + |\Delta|^2}$ , where  $E_\pm = (E_{X_b}^K \pm E_{X_i}^K)/2$ . Clearly, the mixing coefficients depend on the relative energy ordering of  $X_b$  and  $X_i$ , which coincide near  $\epsilon \sim 2.0\%$  [Fig. 1(d)]. For  $E_{X_b} < E_{X_i}$  [Fig. 1(c)], they satisfy  $|C_+^b|^2 =$

$|C_-^i|^2 = \sin^2(\theta/2)$  and  $|C_+^b|^2 = |C_+^i|^2 = \cos^2(\theta/2)$ , with  $\tan \theta = |\Delta|/E_-$ . Particularly, in Regime I [Fig. 1(c);  $\varepsilon < 1.55\%$ ], the lower ( $|-\rangle$ ) and upper ( $|+\rangle$ ) branches are predominantly  $X_i$ -like and  $X_b$ -like, respectively [cf. Figs. 1(c) and 1(d)]. When the energy ordering reverses ( $E_{X_b} > E_{X_i}$ ), the dominant characters of the two hybridized branches interchange—namely, the lower (upper) branch becomes  $X_b$ -like ( $X_i$ -like) in Regime III. Near the crossover point (Regime II), corresponding to  $\varepsilon \sim 2\%$ , the two types of excitons are strongly hybridized, exhibiting comparable  $X_b$  and  $X_i$  character. These features are important for interpreting experimental data in Ref. [11].

We further determine the *nominally mixed* states using the perturbative approach, expressed as  $|X_b\rangle^{\text{mix}} = C_b^b|X_b\rangle + C_b^i|X_i\rangle$  and  $|X_i\rangle^{\text{mix}} = C_i^i|X_i\rangle - C_b^b|X_b\rangle$ , with  $|C_b^b|^2 = |C_i^i|^2 = 4/(4 + \tan^2 \theta)$  and  $|C_b^i|^2 = |C_b^b|^2 = \tan^2 \theta/(4 + \tan^2 \theta)$ . Although both  $|X_b\rangle^{\text{mix}}$  and  $|X_i\rangle^{\text{mix}}$  contain finite admixtures of  $X_b$  and  $X_i$  components, each remains primarily dominated by its own parent state. This behavior contrasts with that of the genuinely hybridized eigenstates ( $|\pm\rangle$ ), whose dominant character continuously interchanges between  $X_b$  and  $X_i$  with strain, as aforementioned. As a consequence, far from the avoided crossing,  $|+\rangle \rightarrow X_i$  and  $|-\rangle \rightarrow X_b$  for  $\varepsilon < 1.55\%$  [Regime I], and  $|+\rangle \rightarrow X_b$  and  $|-\rangle \rightarrow X_i$  for  $\varepsilon < 2.55\%$  [Regime III]. For quantitative comparison of the mixing amplitudes  $C_{\pm}^{b(i)}$  (for  $|\pm\rangle$ ) and  $C_{b(i)}^{b(i)}$  (for  $|X_{b(i)}\rangle^{\text{mix}}$ ), see the SM.

*Excitonic scattering channels and valley dynamics.*— Figure 2(b) shows the intra- and intervalley relaxation channels of both hybridized ( $|\pm\rangle$ ) and nonhybridized ( $X_m$ ,  $X_d$ ) excitonic states under the linearly polarized excitation, which coherently drives the formation of  $X_b$  in both the K ( $\sigma^+$ ) and K' ( $\sigma^-$ ) valleys. We reveal that  $X_b$  can convert into the *opposite-valley* indirect exciton  $X_i^{\Gamma K'}$  through two sequential scattering steps [Fig. 2(a)]: (i) exchange-interaction (EI)-induced intervalley scattering to the higher-energy intermediate state  $X_m$  [29] [channels 3-6 in Fig. 2(b)], followed by (ii) an intravalley spin-flip (SF) relaxation of  $X_m$  into  $X_i^{\Gamma K'}$  (channels 7 and 8). Simultaneously,  $X_b$  couples to  $X_i$  within the same valley via *shared* electronic states [Fig. 1(b) and Eq. (1)], forming hybridized eigenstates  $|\pm\rangle$  that comprise both  $X_b$  [yellow frame in Fig. 2(b)] and  $X_i$  (gray frame) components. Additional relaxation pathways include EI-driven intervalley transfer of  $X_b$  (channels 1 and 2) and nonradiative intravalley bright-dark conversion via SF scattering (channels 9 and 10). Because of the  $B$ -field-induced lifting of valley degeneracy, we consider *asymmetric* intervalley transfer of excitonic states (channels 1-6), with scattering rates [35]  $\gamma_{\pm} = (1/\tau_{i0})[\Gamma^2/(\Gamma^2 + \Delta E^2)] + \alpha\Delta E^3/|e^{\pm\Delta E/k_B T} - 1|$ , where  $\gamma_-$  ( $\gamma_+$ ) describes transitions from the higher (lower) to lower (higher)-energy valley. The first term represents the electron-hole EI contribution, which acts as an in-plane field and drives intervalley excitonic transfer with characteristic timescale  $\tau_{i0}$  and width parameter  $\Gamma$  [35]. The second term accounts for phonon-assisted scattering [36], governed by the exciton-phonon coupling constant  $\alpha$  and the valley Zeeman splitting  $\Delta E$ . With the above considerations, we obtain the coupled valley dynamic equations, which for hybridized

states  $|\pm\rangle$  in the K valley read,

$$\frac{dn_+}{dt} = -|C_+^b|^2 g - \frac{n_+}{\tau_+} - \frac{|C_+^b|^2 n_+}{1/\Gamma_9^{b \Rightarrow d}} + \frac{n_d}{1/\Gamma_9^{d \Rightarrow b}} - \frac{|C_+^b|^2 n_+}{1/\gamma_1} + \frac{|C_+^b|^2 n'_+}{1/\gamma'_1} - \frac{|C_+^b|^2 n_+}{1/\gamma_3} + \frac{n'_m}{1/\gamma'_3} - \frac{|C_+^i|^2 n_+}{1/\Gamma_7^{i \Rightarrow m}} + \frac{n_m}{1/\Gamma_7^{m \Rightarrow i}}, \quad (4)$$

$$\frac{dn_-}{dt} = -|C_-^b|^2 g - \frac{n_-}{\tau_-} - \frac{|C_-^b|^2 n_-}{1/\Gamma_{10}^{b \Rightarrow d}} + \frac{n_d}{1/\Gamma_{10}^{d \Rightarrow b}} - \frac{|C_-^b|^2 n_-}{1/\gamma_2} + \frac{|C_-^b|^2 n'_-}{1/\gamma'_2} - \frac{|C_-^b|^2 n_-}{1/\gamma_6} + \frac{n'_m}{1/\gamma'_6} - \frac{|C_-^i|^2 n_-}{1/\Gamma_8^{i \Rightarrow m}} + \frac{n_m}{1/\Gamma_8^{m \Rightarrow i}}, \quad (5)$$

where  $n_{\pm}$ ,  $n_d$ , and  $n_m$  denote the K-valley densities of  $|\pm\rangle$ ,  $X_d$ , and  $X_m$ , respectively. And,  $\gamma_{1-6}$  ( $\gamma'_{1-6}$ ) represent the intervalley scattering rates of excitonic states from the K (K') to the K' (K) valley, with the subscripts indicating the channels 1-6 in Fig. 2. Similarly,  $\Gamma_{7-10}^{A \Rightarrow B}$  denote the scattering rates of the intravalley scattering channels 7-10 within the K valley, where A  $\Rightarrow$  B indicates excitonic transfer from  $X_A$  to  $X_B$  with  $A(B) \in i, m, b, d$ . For the valley dynamics of remaining excitonic states and those in the K' valley and relevant parameters used in our calculations, see the SM (Secs. III and IV).

*Optical activation of hybridized  $\Gamma - K$  indirect dark excitons.*— According to experimental reports in Ref. [11] [shaded (colored) regions in Fig. 1(e)], the PL response evolves systematically with strain. Specifically, for  $\varepsilon < 1.6\%$  (purple), the PL arises almost exclusively from the direct exciton  $X_b$ . At  $\varepsilon = 2.4\%$  (green), both the direct and indirect branches become visible, with  $X_b$  showing slightly stronger emission. When the strain increases to  $3.2\%$  (pink), the PL is dominated by  $X_i$ , with the direct excitonic contribution nearly vanishing. Our theory clarifies that the microscopic origin of the strain evolution arises from the hybridized eigenstates  $|\pm\rangle$ , rather than from the *nominally mixed* perturbative states  $|X_{b(i)}\rangle^{\text{mix}}$  [Fig. 1(g)]. Particularly, for  $\varepsilon = 3.2\%$ , the emission primarily originates from  $|+\rangle$  state, which is dominated by the  $X_b$  component (similar to the low-strain case), in stead of by the  $X_i$  component. Below we analyze the underlying physics.

At small strain,  $X_b$  lies substantially below  $X_i$  [Fig. 1(d)] owing to the much lower VB maximum at  $\Gamma$  valley relative to K valley. Consequently,  $|-\rangle$  and  $|+\rangle$  are almost purely  $X_b$ - and  $X_i$ -like, respectively [Regime I in Fig. 1(c)], and only the  $X_b$ -dominated  $|-\rangle$  branch emits efficiently, giving rise to the observed single-peak PL at  $\varepsilon < 1.6\%$ , in full agreement with experiment [Fig. 1(e)]. This scenario behaves as a conventional direct-exciton emitter, with the indirect component being energetically inaccessible for radiative recombination.

As strain increases, the energy detuning between  $X_b$  and  $X_i$  shrinks, strengthening their coupling and causing the  $|+\rangle$  branch to acquire increasing  $X_b$  content [cf. Figs. 1(c) and 1(d)]. Once the strain approaches  $\varepsilon \simeq 2.0\%$ , the two types of bare excitons become nearly degenerate, and the system enters the strongly hybridized scenario [Regime II in Fig. 1(c)], giving rise to pronounced avoided crossing. Note that, across this anticrossing, the dominant characters of  $|-\rangle$  and  $|+\rangle$  interchange. This explains why, at  $\varepsilon = 2.4\%$ , both emission

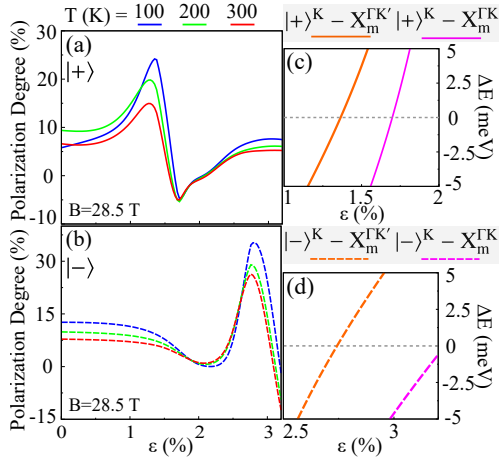


Figure 3. (Color online) (a), (b) Valley polarization of  $|\pm\rangle$  versus strain at  $T = 100, 200, 300$  K. (c), (d) Energy separation  $\Delta E_{\pm,m}^{\tau} = E_{|\pm\rangle}^{\text{K}} - E_{X_m}^{\text{K'}}$  between  $|\pm\rangle$  in the K valley and the intermediate state  $X_m^{\text{K'}}$  (K valley) and  $X_m^{\text{K}}$  (K' valley) as functions of strain.

branches appear with comparable intensity: the  $|+\rangle$  state has gained substantial direct-exciton weight, while  $|-\rangle$  has begun to lose it. The small energy splitting (only a few meV) further equalizes their thermal populations, so that the  $|+\rangle$  state has slight stronger PL intensity than  $|-\rangle$  state.

At even higher strain [Regime III], e.g.,  $\varepsilon = 3.2\%$ , the  $|+\rangle$  state dominates the PL emission despite belonging to the higher-energy branch, since it is predominantly  $X_b$ -derived. Thus, the observed PL does not come from the nominal perturbative state  $|X_i\rangle^{\text{mix}}$ —which would be  $X_i$ -like—but from the genuinely hybridized eigenstate whose character continuously evolves across the avoided crossing. The shaded (gray) region ( $\varepsilon = 1.55\text{--}2.55\%$ ) in Fig. 1(g) marks the strain range where the hybridization is sufficiently strong that the nominally mixed states lose physical meaning.

Figure 1(f) shows that the intermediate exciton  $X_m$  plays a crucial role in shaping the PL distribution. Without  $X_m$  in the relaxation channels, the  $|-\rangle$  branch would dominate the PL at all strain values, in clear contradiction with experiment. Including  $X_m$  introduces a relaxation bottleneck that selectively blocks population flow from  $|+\rangle$  to  $|-\rangle$ , thereby stabilizing the occupation of the upper hybridized state in the relevant strain window. This routing effect of  $X_m$  is essential for reproducing both the enhancement of PL of the  $|+\rangle$  state at high strain and the correct strain evolution of the two-peak PL structure.

*“Sinusoidal” valley control.*— Beyond reproducing the measured PL spectra, our model reveals a striking and highly strain-sensitive valley polarization (VP) response of the hybridized excitons [Figs. 3(a) and 3(b)], demonstrating that strain acts not merely as an energy shifter but as a powerful and versatile control knob for valley physics.

For the upper branch  $|+\rangle$  [Fig. 3(a)], the VP shows a pronounced nonmonotonic “sinusoidal”-like evolution that encodes the interplay among direct–indirect hybridization, intervalley pathways, and the intermediate state  $X_m$ . Specifically,

at small strain,  $|+\rangle$  is predominantly  $X_i$ -like, and intravalley relaxation through channel 7 dominates. Because the intermediate state  $X_m$  lies above  $|+\rangle$  in both valleys—but with a larger detuning in K than in K’—the resulting imbalance favors excitonic population in the K valley, yields a *positive* VP that increases with strain. Around  $\varepsilon \sim 1.3\%$ ,  $X_m^{\text{K'}}$  becomes nearly resonant with  $|+\rangle$  [Fig. 3(c)], greatly enhancing the direct–indirect mixing. Then, the intervalley scattering through channel 3 takes over the dominance and preferentially transfers  $X_b$  population the K valley to  $X_m$  of the K’ valley, suppressing the VP and even driving it negative for  $1.3\% \lesssim \varepsilon \lesssim 1.7\%$ .

At even larger strain, the  $|+\rangle$  state rises above both  $X_m^{\text{K}}$  and  $X_m^{\text{K'}}$  [Fig. 3(c)], activating scattering channel 4 and restoring an increasing VP trend with strain. The resulting “sinusoidal”-like VP profile, with its reversible sign switch, constitutes a continuously tunable *valley dial*, offering deterministic, analog-like control over the valley degree of freedom, far exceeds binary (on/off) control schemes. Importantly, we verify that this “sinusoidal” pattern is basically resilient against both thermal (temperature) [Fig. 3(a)] and magnetic [See the SM; Fig. S2] effects, underscoring its suitability for realistic device operation. We emphasize that this mechanism is fundamentally distinct from the dark-exciton—assisted biexciton VP reversals in Ref. [37]: here the effect arises from coherent direct–indirect excitonic hybridization mediated by an intermediate state  $X_m$ , not from higher-order excitonic complexes.

The lower branch  $|-\rangle$  [Fig. 3(b)] shows a markedly different strain evolution, underscoring the selective and *state-specific* nature of strain control. At small strain,  $|-\rangle$  is largely  $X_b$ -derived; channel 2 governs relaxation, while channels 5 and 6 are suppressed, because  $X_m$  lies far above  $|-\rangle$  [Fig. 3(d)] and the valley splitting is sizable. Consequently, the VP is nearly strain-insensitive for  $\varepsilon \lesssim 1\%$ . As strain exceeds  $\sim 1\%$ , the valley splitting of  $|-\rangle$  diminishes, enabling enhanced intervalley transfer and reducing VP up to  $\varepsilon \sim 2\%$ . For  $2\% < \varepsilon < 2.7\%$ , the EI-assisted intervalley transfer through channel 6 partially restores the VP. At even larger strain ( $\varepsilon \gtrsim 2.7\%$ ), channel 5 becomes dominant, strengthening intervalley transfer and driving the VP downward again. The contrasted responses of the upper and lower hybridized branches demonstrate that strain can potentially selectively address individual excitonic eigenstates, enabling level-resolved selective valley control.

*Concluding remarks.*— Our work resolves the fundamental obstacle in understanding momentum-indirect  $\Gamma$  – K excitons and establishes the first unified framework that quantitatively reproduces strain-tunable PL in experiments. By revealing the true PL-active hybridized eigenstates, identifying a previously unrecognized intermediate exciton, and constructing a two-step direct–indirect conversion mechanism, we clarify the microscopic origin of indirect PL. Notably, we propose a new concept of strain-driven “sinusoidal” valley control, providing a continuously tunable and highly sensitive *valley dial* far beyond binary switching. Together with the nearly opposite magnetic-field responses of the two hybridized branches (SM; Sec. IV), our results provide a robust and practical framework for accessing and manipulat-

ing long-lived indirect excitons, and open new avenues toward programmable valley pseudospin engineering and next-generation valleytronic quantum technologies. As a final remark, our work also offers concrete predictions for forthcoming experiments—especially in light of the very recent strain-controlled VP observations for indirect Q – K excitons [12].

**Acknowledgments.**— We would like to thank Paulo Eduardo de Faria Junior and Zhichu Chen for valuable comments. We also wish to acknowledge the late Fanyao Qu, whose generosity in sharing his BSE calculations and whose scientific spirit continue to be warmly remembered. This work was supported by the National Natural Science Foundation of China (Grants No. 12274256, No. 11874236, No. 12022413, No. 11674331, and No. 61674096), the Major Basic Program of Natural Science Foundation of Shandong Province (Grant No. ZR2021ZD01), the National Key R&D Program of China (Grant No. 2022YFA1403200), and the “Strategic Priority Research Program (B)” of the Chinese Academy of Sciences (Grant No. XDB33030100).

---

\* yongjf@qfnu.edu.cn

- [1] G. Wang, A. Chernikov, M. M. Glazov, T. F. Heinz, X. Marie, T. Amand, and B. Urbaszek, Colloquium: Excitons in atomically thin transition metal dichalcogenides, *Rev. Mod. Phys.* **90**, 021001 (2018).
- [2] M. Koperski, M. R. Molas, A. Arora, K. Nogajewski, A. O. Slobodeniuk, C. Faugeras, and M. Potemski, Optical properties of atomically thin transition metal dichalcogenides: observations and puzzles, *Nanophotonics* **6**, 1289 (2017).
- [3] S. Mouri, Y. Miyauchi, M. Toh, W. Zhao, G. Eda, and K. Matsuda, Nonlinear photoluminescence in atomically thin layered WSe<sub>2</sub> arising from diffusion-assisted exciton-exciton annihilation, *Phys. Rev. B* **90**, 155449 (2014).
- [4] A. C. Dias, J. Fu, L. Villegas-Lelovsky, and F. Qu, Robust effective zeeman energy in monolayer MoS<sub>2</sub> quantum dots, *Journal of Physics: Condensed Matter* **28**, 375803 (2016).
- [5] H. Yu, X. Cui, X. Xu, and W. Yao, Valley excitons in two-dimensional semiconductors, *National Science Review* **2**, 57 (2015).
- [6] H. Yu, G.-B. Liu, P. Gong, X. Xu, and W. Yao, Dirac cones and dirac saddle points of bright excitons in monolayer transition metal dichalcogenides, *Nat. Commun.* **5**, 3876 (2014).
- [7] M. Baranowski, A. Surrente, D. K. Maude, M. Ballottin, A. A. Mitioglu, P. C. M. Christianen, Y. C. Kung, D. Dumcenco, A. Kis, and P. Plochocka, Dark excitons and the elusive valley polarization in transition metal dichalcogenides, *2D Materials* **4**, 025016 (2017).
- [8] J. P. Echeverry, B. Urbaszek, T. Amand, X. Marie, and I. C. Gerber, Splitting between bright and dark excitons in transition metal dichalcogenide monolayers, *Phys. Rev. B* **93**, 121107 (2016).
- [9] T. Yu and M. W. Wu, Valley depolarization due to intervalley and intravalley electron-hole exchange interactions in monolayer MoS<sub>2</sub>, *Phys. Rev. B* **89**, 205303 (2014).
- [10] F. Volmer, S. Pissinger, M. Ersfeld, S. Kuhlen, C. Stampfer, and B. Beschoten, Intervalley dark trion states with spin lifetimes of 150 ns in WSe<sub>2</sub>, *Phys. Rev. B* **95**, 235408 (2017).
- [11] E. Blundo, P. E. F. Junior, A. Surrente, G. Pettinari, M. A. Prosnikov, K. Olkowska-Pucko, K. Zollner, T. Woźniak, A. Chaves, T. Kazimierczuk, M. Felici, A. Babiński, M. R. Molas, P. C. M. Christianen, J. Fabian, and A. Polimeni, Strain-induced exciton hybridization in ws<sub>2</sub> monolayers unveiled by zeeman-splitting measurements, *Phys. Rev. Lett.* **129**, 067402 (2022).
- [12] A. M. Kumar, D. J. Bock, D. Yagodkin, E. Wietek, B. Höfer, M. Sinner, A. Dewambrecies, P. H. López, S. Kovalchuk, R. Dhingra, S. Heeg, C. Gahl, F. Libisch, A. Chernikov, E. Malic, R. Rosati, and K. I. Bolotin, Strain control of valley polarization dynamics in a 2D semiconductor via exciton hybridization, *Nano Lett.* **25**, 15164 (2025).
- [13] P. E. Faria Junior, K. Zollner, T. Woźniak, M. Kurpas, M. Gmitra, and J. Fabian, First-principles insights into the spin-valley physics of strained transition metal dichalcogenides monolayers, *New J. Phys.* **24**, 083004 (2022).
- [14] A. M. Kumar, D. Yagodkin, R. Rosati, D. J. Bock, C. Schattauer, S. Tobisch, J. Hagel, B. Höfer, J. N. Kirchhof, P. Hernández López, K. Burfeindt, S. Heeg, C. Gahl, F. Libisch, E. Malic, and K. I. Bolotin, Strain fingerprinting of exciton valley character in 2d semiconductors, *Nat. Commun.* **15**, 7546 (2024).
- [15] E. Henríquez-Guerra, H. Li, P. Pasqués-Gramage, D. Gosálbez-Martínez, R. D’Agosta, A. Castellanos-Gómez, and M. R. Calvo, Large biaxial compressive strain tuning of neutral and charged excitons in single-layer transition metal dichalcogenides, *ACS Appl. Mater. Interfaces* **15**, 57369 (2023).
- [16] E. Stellino, B. D’Alò, E. Blundo, P. Postorino, and A. Polimeni, Fine-tuning of the excitonic response in monolayer ws<sub>2</sub> domes via coupled pressure and strain variation, *Nano Lett.* **24**, 3945 (2024).
- [17] K. F. Mak, K. L. McGill, J. Park, and P. L. McEuen, The valley hall effect in mos<sub>2</sub> transistors, *Science* **344**, 1489 (2014).
- [18] D. Xiao, G.-B. Liu, W. Feng, X. Xu, and W. Yao, Coupled spin and valley physics in monolayers of mos<sub>2</sub> and other group-vi dichalcogenides, *Phys. Rev. Lett.* **108**, 196802 (2012).
- [19] Q. H. Wang, K. Kalantar-Zadeh, A. Kis, J. N. Coleman, and M. S. Strano, Electronics and optoelectronics of two-dimensional transition metal dichalcogenides quantum dots, *Nat. Nanotechnol.* **7**, 699 (2012).
- [20] K. Kośmider, J. W. González, and J. Fernández-Rossier, Large spin splitting in the conduction band of transition metal dichalcogenide monolayers, *Phys. Rev. B* **88**, 245436 (2013).
- [21] W. Hsu, L. Lu, D. Wang, J. Huang, M. Li, T. Chang, Y. Chou, Z. Jiang, H. Jeng, L. Li, and W. Chang, Evidence of indirect gap in monolayer wse<sub>2</sub>, *Nat. Commun.* **8**, 929 (2017).
- [22] F. Wu, F. Qu, and A. H. MacDonald, Exciton band structure of monolayer MoS<sub>2</sub>, *Phys. Rev. B* **91**, 075310 (2015).
- [23] A. C. Dias, H. Bragança, H. Zeng, A. L. A. Fonseca, D.-S. Liu, and F. Qu, Large room-temperature valley polarization by valley-selective switching of exciton ground state, *Phys. Rev. B* **101**, 085406 (2020).
- [24] G.-H. Peng, P.-Y. Lo, W.-H. Li, Y.-C. Huang, Y.-H. Chen, C.-H. Lee, C.-K. Yang, and S.-J. Cheng, Distinctive signatures of the spin- and momentum-forbidden dark exciton states in the photoluminescence of strained WSe<sub>2</sub> monolayers under thermalization, *Nano Lett.* **19**, 2299 (2019).
- [25] R. Tempelaar and T. C. Berkelbach, Many-body simulation of two-dimensional electronic spectroscopy of excitons and trions in monolayer transition metal dichalcogenides, *Nat. Commun.* **10**, 3419 (2019).
- [26] X. Jiang, Q. Zheng, Z. Lan, W. A. Saidi, X. Ren, and J. Zhao, Real-time GW-bse investigations on spin-valley exciton dynamics in monolayer transition metal dichalcogenide, *Sci. Adv.*

7, 3759 (2021).

[27] E. Ridolfi, D. Le, T. S. Rahman, E. R. Mucciolo, and C. H. Lewenkopf, A tight-binding model for mos<sub>2</sub> monolayers, *J. Phys.: Condens. Matter* **27**, 365501 (2015).

[28] A. C. Dias, F. Qu, D. L. Azevedo, and J. Fu, Band structure of monolayer transition-metal dichalcogenides and topological properties of their nanoribbons: Next-nearest-neighbor hopping, *Phys. Rev. B* **98**, 075202 (2018).

[29] Strictly speaking, the momentum mismatch between the  $\Gamma$  and K valleys endows the intermediate exciton with a finite center-of-mass momentum, so the first conversion step may rely on phonon-assisted exchange scattering [9].

[30] G. Aivazian, Z. Gong, A. M. Jones, J. Yan, D. G. Mandrus, C. Zhang, D. Cobden, W. Yao, and X. Xu, Magnetic control of valley pseudospin in monolayer wse<sub>2</sub>, *Nat. Phys.* **11**, 148 (2015).

[31] T. Woźniak, P. E. Faria Junior, G. Seifert, A. Chaves, and J. Kunstmann, Exciton *g* factors of van der waals heterostructures from first-principles calculations, *Phys. Rev. B* **101**, 235408 (2020).

[32] L. M. Roth, B. Lax, and S. Zwerdling, Theory of optical magneto-absorption effects in semiconductors, *Phys. Rev.* **114**, 90 (1959).

[33] D. V. Rybkovskiy, I. C. Gerber, and M. V. Durnev, Atomically inspired  $k \cdot p$  approach and valley zeeman effect in transition metal dichalcogenide monolayers, *Phys. Rev. B* **95**, 155406 (2017).

[34] P. E. Faria Junior, M. Kurpas, M. Gmitra, and J. Fabian,  $k \cdot p$  theory for phosphorene: Effective *g*-factors, landau levels, and excitons, *Phys. Rev. B* **100**, 115203 (2019).

[35] A. Surrente, Ł. Kłopotowski, N. Zhang, M. Baranowski, A. A. Mitioglu, M. V. Ballottin, P. C. Christianen, D. Dumcenco, Y.-C. Kung, D. K. Maude, A. Kis, and P. Plochocka, Intervalley scattering of interlayer excitons in a MoS<sub>2</sub>/MoSe<sub>2</sub>/MoS<sub>2</sub> heterostructure in high magnetic field, *Nano Lett.* **18**, 3994 (2018).

[36] R. Orbach, Spin-lattice relaxation in rare-earth salts, *Proceedings of the Royal Society of London. Series A. Mathematical and Physical Sciences* **264**, 458 (1961).

[37] P. Nagler, M. V. Ballottin, A. A. Mitioglu, M. V. Durnev, T. Taniguchi, K. Watanabe, A. Chernikov, C. Schüller, M. M. Glazov, P. C. Christianen, and T. Korn, Zeeman splitting and inverted polarization of biexciton emission in monolayer WS<sub>2</sub>, *Phys. Rev. Lett.* **121**, 057402 (2018).